Journal of Magnetic Resonance 310 (2020) 106636

Contents lists available at ScienceDirect

Journal of Magnetic Resonance

journal homepage: www.elsevier.com/locate/jmr

Using the heteronuclear Bloch-Siegert shift of protons for B_1 calibration of insensitive nuclei not present in the sample

Ivan Hung, Peter Gor'kov, Zhehong Gan

National High Magnetic Field Laboratory, 1800 East Paul Dirac Drive, Tallahassee, FL 32310, USA

ARTICLE INFO

Article history:
Received 7 October 2019
Revised 24 October 2019
Accepted 26 October 2019
Available online 28 October 2019

Keywords:
Bloch-Siegert shift
Stark shift
Rotating wave approximation
Counter rotating wave
Circular *rf* field
Floquet theory
Perturbation theory
rf field calibration
B_1 field
Indirect detection
Full-echo

ABSTRACT

Indirect *rf* field calibration using the heteronuclear Bloch-Siegert shift is presented. This method is useful for calibrating $\omega_1 = -\gamma B_1$ for the *rf* channels of small volume fast-spinning probes on which direct *rf* calibration is practically inconvenient or difficult for insensitive low-γ nuclei. Proton signals are observed for the *rf* calibration of the insensitive nuclei without requiring their presence in the sample. For a linearly modulated *rf* field, the heteronuclear Bloch-Siegert shift is given by, $\Delta\omega_{BS} = \omega_0\omega_1^2/(\omega_0^2 - \omega_{\text{irr}}^2)$, where ω_0 and ω_{irr} are the Larmor and irradiation frequencies, respectively. A short protocol using full-echo acquisition of protons is described for measurement of the phase change induced by the Bloch-Siegert shift. The calibration procedure is validated by a comparison with direct ^{13}C calibration and demonstrated for ^{14}N *rf* field measurement of a 0.75 mm 100 kHz triple-resonance magic-angle spinning probe.

1. Introduction

Most of NMR experiments nowadays employ multiple *rf* channels and pulses at different frequencies to cover multiple nuclei of interest with both on- and off-resonance irradiation. Before the detection of magnetic resonance, the paper by Bloch and Siegert about the rotating wave approximation (RWA) in 1940 [1] predicted that the off-resonance counter-rotating circular component of *cw* irradiation can induce a small shift $\Delta\omega_{BS} = \omega_1^2/(4\omega_0)$, where $\omega_0 = -\gamma B_0$ is the Larmor frequency from the main magnetic field, $\omega_1 = -\gamma B_1$ is the Rabi frequency from the *rf* field, and γ is the gyromagnetic ratio. For double-resonance experiments, a similar kind of shift occurs when *rf* irradiation is applied at a frequency ω_{irr} far from the resonance frequency ω_0. The shift in this case shares the origin of the AC Stark effect $\Delta\omega_{ACStark} = \omega_1^2/[2(\omega_0 - \omega_{\text{irr}})]$ in microwave spectroscopy [2,3], but has since been known as the Bloch-Siegert shift in magnetic resonance spectroscopy. The Bloch-Siegert shift is usually small given the large magnitude difference between ω_0 and ω_1, but can become larger when ω_0 and ω_{irr} get closer [4] and more profound for homonuclear near-resonance conditions, such as for homonuclear *J* decoupling [5], solvent suppression [6], and selective shaped pulses [7,8]. The direct relation of the Bloch-Siegert shift to $\omega_1 = -\gamma B_1$ also allows calibration of the *rf* field strength [9] and mapping of the B_1 field in magnetic resonance imaging [10].

Here we propose the use of the Bloch-Siegert shift for indirect *rf* calibration of insensitive low-γ nuclei via proton detection. This work is triggered by the recent completion of a triple-resonance 0.75 mm 100 kHz magic-angle spinning (MAS) probe at the National High Magnetic Field Laboratory, and the development of ultrafast MAS for proton-detected solid-state NMR. Ultrafast spinning is critical for narrowing proton resonances and prolonging T_2 relaxation of solids, but comes at the expense of small rotors with very limited sample space. Calibrating the *rf* field for channels other than the ^{1}H channel becomes difficult due to small sample volume (~290 nL in this case), and the intrinsically weak signals from low-γ nuclei. Calibrating the *rf* field without actually observing the insensitive nuclei of interest also becomes advantageous because a single experimental setup with ^{1}H detection can be used to calibrate virtually all nuclei and *rf* channels on the probe. The practical inconvenience of packing/unpacking and keeping many setup samples in small rotors can also be avoided.

In the following, we first revisit the Bloch-Siegert effect following the work by Shirley and others [11,12]. The use of Floquet

E-mail address: gan@magnet.fsu.edu (Z. Gan)

https://doi.org/10.1016/j.jmr.2019.106636
1090-7807/

theorem treats all cases in terms of frequency offsets, and *rf* fields with linear or circular modulation. The case of heteronuclear irradiation with a linearly modulated *rf* will be used for indirect *rf* calibration through proton detection. The Bloch-Siegert shift can be measured by the induced phase change accumulated over a spin-echo. Hence, a protocol for acquiring full-echo signals, data processing, and spectral phasing is described for measuring the phase change precisely. Indirect *rf* calibration is demonstrated for the ^{14}N channel of the triple-resonance 0.75 mm MAS probe after validation with direct ^{13}C measurements on [U-^{13}C, ^{15}N]L-alanine.

2. Theory

The Hamiltonian of a spin placed in a strong magnetic field and under *rf* irradiation consists of the Zeeman interaction and the time-dependent *rf* Hamiltonian

$$H = \omega_0 S_z + 2\gamma B_1 S_x \cos(\omega_{\text{irr}} t + \varphi) \tag{1}$$

For the *rf* Hamiltonian, we have neglected the longitudinal component and assumed the *x*-axis for the direction of the transverse B_1 field, which has frequency ω_{irr} and phase φ. Floquet theory transfers the time-dependent problem into a time-independent one [11]. Solving the eigenvalue problem of the Floquet Hamiltonian yields an effective Hamiltonian. The difference between the effective Hamiltonian and the Zeeman interaction is then the Bloch-Siegert shift induced by the *rf* irradiation.

The explicit matrix of the Floquet Hamiltonian shows non-zero elements in blocks separated by the Floquet index $n_F = +1, 0, -1$ (only three are shown),

$$H_F = \begin{pmatrix} \begin{vmatrix} \frac{\omega_0}{2}+\omega_{\text{irr}} & \\ & -\frac{\omega_0}{2}+\omega_{\text{irr}} \end{vmatrix} & \begin{vmatrix} & \frac{\omega_1}{2} \\ \frac{\omega_1}{2} & \end{vmatrix} & \\ \begin{vmatrix} & \frac{\omega_1}{2} \\ \frac{\omega_1}{2} & \end{vmatrix} & \begin{vmatrix} \frac{\omega_0}{2} & \\ & -\frac{\omega_0}{2} \end{vmatrix} & \begin{vmatrix} & \frac{\omega_1}{2} \\ \frac{\omega_1}{2} & \end{vmatrix} \\ & \begin{vmatrix} & \frac{\omega_1}{2} \\ \frac{\omega_1}{2} & \end{vmatrix} & \begin{vmatrix} \frac{\omega_0}{2}-\omega_{\text{irr}} & \\ & -\frac{\omega_0}{2}-\omega_{\text{irr}} \end{vmatrix} \end{pmatrix} \tag{2}$$

The upper and lower blocks across the diagonal represent two circularly counter rotating components of the linearly modulated *rf* field,

$$2\gamma B_1 S_x \cos(\omega_{\text{irr}} t + \varphi) = \omega_1 \left[e^{i(\omega_{\text{irr}} t+\varphi)} + e^{-i(\omega_{\text{irr}} t+\varphi)}\right](S_+ + S_-) \tag{3}$$

To derive the Bloch-Siegert shift, we can set the *rf* phase $\varphi = 0$ without loss of generality.

In order to solve the eigenvalue problem of the Floquet Hamiltonian, perturbation theory or more explicitly pair-wise Jacobi transformation [13] is applied to eliminate off-diagonal elements. The elimination introduces a small perturbation to the diagonal elements. The matrix in Eq. (2) shows that each state is perturbed only by two pairs of off-diagonal elements from the *rf* irradiation. Once the matrix is diagonalized, the center block becomes the effective Hamiltonian and is used to derive the Bloch-Siegert shift.

Let us first consider the original Bloch-Siegert shift with an irradiation frequency matching the Larmor frequency $\omega_{\text{irr}} = \omega_0$. In this case, one pair of *rf* field elements connects the two degenerate energy levels $(-\omega_0/2) + \omega_{\text{irr}}$ and $\omega_0/2$ with $\Delta n_F = +1$.The match of frequencies drives the resonance effectively and induces transitions between the two states. The other pair of *rf* elements connect the $\omega_0/2$ and $(-\omega_0/2) - \omega_{\text{irr}}$ energy levels separated by $2\omega_0$. This counter-rotating component is ineffective in driving the resonance (i.e., the rotating wave approximation), but can cause a small change to the energy levels equal to $\omega_1^2/8\omega_0$. Bloch and Siegert predicted a shift of the transition frequency between the two energy levels $+\omega_0/2$ and $-\omega_0/2$ in the center block by

$$\Delta\omega_{BS} = \frac{\omega_1^2}{4\omega_0} \tag{4}$$

This case is rarely observed nowadays in pulsed Fourier-Transform NMR as *rf* irradiation at the Larmor frequency is usually turned off during acquisition of the free induction decay (FID).

Second, we consider an irradiation frequency ω_{irr} far from the Larmor frequency ω_0 of the observed nucleus, i.e., $|\omega_0 - \omega_{\text{irr}}| \gg \omega_1$; the case we will use for indirect *rf* calibration. In this case, none of the two rotating components of the linearly modulated *rf* field drives the resonance, but both contribute to a separation between the two energy-levels

$$\Delta\omega_{BS} = \frac{\omega_1^2}{2(\omega_0 - \omega_{\text{irr}})} + \frac{\omega_1^2}{2(\omega_0 + \omega_{\text{irr}})} = \frac{\omega_0\omega_1^2}{\omega_0^2 - \omega_{\text{irr}}^2} \tag{5}$$

Each of the two terms above correspond to the AC Stark shift from one of the circular components of a linearly modulated *rf* field [2]. The Bloch-Siegert terminology is kept in use here for this type of effect in magnetic resonance.

The Bloch-Siegert shift is usually small as $|\omega_0 \pm \omega_{\text{irr}}| \gg \omega_1$, but becomes more significant when *rf* irradiation gets closer to resonance. In this case, we can neglect the smaller $\omega_1^2/[2(\omega_0 + \omega_{\text{irr}})]$ term leaving only

$$\Delta\omega_{BS} = \frac{\omega_1^2}{2\Delta\omega}, \quad \Delta\omega = \omega_0 - \omega_{\text{irr}} \tag{6}$$

This is the common case of Bloch-Siegert shift observed in selective homonuclear decoupling experiments. The near-resonance case is also used for B_1 field mapping in magnetic resonance imaging [10]. It is noteworthy that the direction of the Bloch-Siegert shift can be upfield or downfield depending on if the ω_{irr} is above or below the observed peak frequency, respectively. The peaks always shift away from the irradiating frequency.

The effective *rf* field in the rotating frame is often used to derive the Bloch-Siegert shift. In the rotating frame, the magnetization vector rotates about the effective field at a frequency equal to its magnitude, $\omega_{1\text{eff}} = \sqrt{\omega_1^2 + (\omega_0 - \omega_{\text{irr}})^2}$. The near-resonance expression for the Bloch-Siegert shift can be derived by adding $\omega_{1\text{eff}}$ to ω_{irr}. The summed frequency should be equal to the Larmor frequency plus the Bloch-Siegert shift [1,3,10],

$$\omega_0 + \Delta\omega_{BS} = \omega_{\text{irr}} + \sqrt{\omega_1^2 + (\omega_0 - \omega_{\text{irr}})^2} \tag{7}$$

The equation above leads to the same expression as in Eq. (6) for the near-resonance condition. In comparison, despite being more complicated analytically, the use of Floquet theory is capable of treating all cases in one framework with a direct derivation in the laboratory frame.

The second half of the theory is about full-echo signals, more specifically, the data processing and spectral phasing used to measure the change in phase induced by the Bloch-Siegert shift. As illustrated in Fig. 1a, Fourier-transform NMR typically acquires FIDs immediately after excitation. The decaying signal is the same as a spin-echo acquired from the top of the echo, thus it is denoted here as a half-echo. The frequency-domain spectrum is a well-known mixture of absorptive and dispersive line shapes. The desired absorptive spectrum is obtained by spectral phasing. First-order phasing (PHC1) corrects for the delay between excitation and the first recorded data point; a delay necessary due to the probe dead time and transmit/receive (T/R) switching. Band-pass signal filtration and even changes in cable length can also contribute to this delay. The zeroth-order phase correction (PHC0) compensates for all phase delays for *rf* transmission from the

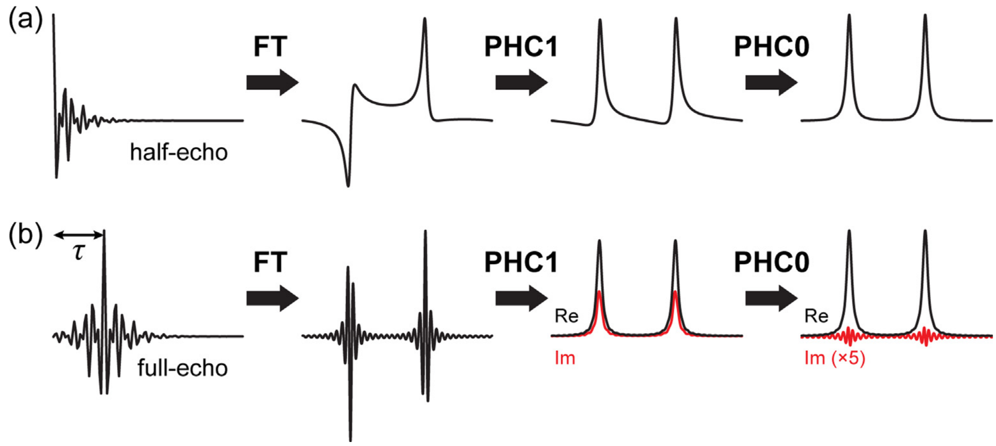

Fig. 1. Illustration of phase correction for (a) half-echo and (b) full-echo time-domain signals. For a full-echo signal, the imaginary part (red traces) of the spectrum is null when properly phased. (For interpretation of the references to colour in this figure legend, the reader is referred to the web version of this article.)

NMR console to the probe, and signal reception from the probe back to the console. The phase correction is usually based on visual adjustment to the absorptive peaks, which can be ambiguous especially with broad and non-symmetric line shapes.

Fig. 1b shows a full-echo signal, which can be related to the half-echo FID by a shift of the origin of the time axis. The decaying half on the right of the full-echo is equal to the half-echo FID, while the rising half of the signal is simply its time reversal and complex conjugate,

$$S(t+\tau) = S(\tau - t)^* \tag{8}$$

Shifting of the time-domain signal can be done equivalently, and more conveniently, in the frequency-domain by applying a first-order phase correction PHC1 = 360° $\times$ n_{dw}, where n_{dw} is the number of dwell intervals between the start of data collection and the top of the full-echo signal, $n_{dw} = \tau/dw$. Eq (8) implies that the imaginary component of a properly phased full-echo signal is zero because

$$\int_{-\infty}^{\tau} S(t)e^{-i\omega t}dt = \int_{\tau}^{\infty} \left[S(t)e^{-i\omega t}\right]^* dt \tag{9}$$

In effect as illustrated in Fig. 1b, the zeroth-order phase only distributes the signal intensity amongst the real and imaginary full-echo spectra, instead of mixing absorptive and dispersive components as for half-echo signals. It is much less ambiguous to null the intensity of full-echo spectra than to adjust the line shape of a half-echo signal so that it is purely absorptive. Hence, we recommend the use of full-echo spectra to measure the signal phase change induced by the Bloch-Siegert effect. It should be noted the full-echo acquisition and the spectral processing have been used in shifted-echo multiple-quantum magic-angle spinning (MQMAS) [14] and dynamic-angle spinning (DAS) [15] experiments.

3. Experimental

Experiments were carried out at 800.1 MHz for ^1H, 201.2 MHz for ^{13}C, and 57.8 MHz for ^{14}N using a 800 MHz Bruker Avance III HD spectrometer. The sample of [U-^{13}C, ^{15}N]-L-alanine was purchased from Aldrich and spun at 95 kHz MAS on a 0.75 mm MAS probe developed at the NHMFL using a spinning assembly and rotors provided by JEOL. In all cases the Bloch-Siegert effect was measured using a ^1H spin-echo ($\pi/2$ – τ_e – π – de – acq) with $\tau_e = 521/\nu_r$ or 5.5 ms, de = 2 ms, and 2 s recycle delay.

4. Results and discussion

Fig. 2 shows the pulse sequence used for indirect *rf* field calibration. The *rf* pulse for the low-γ channel τ_p is applied during the first half of the spin-echo, while the second half allows full-echo acquisition of the proton signal. A spin-echo lasting several milliseconds is typically used. With echo delays limited by T_2 relaxation, there can be some truncation at the beginning of the echo signal. It is also possible for samples with long T_1 relaxation that some residual signals appear at the beginning of the acquisition due to incomplete filtration of signals excited by the refocusing pulse with insufficient recycle delays. This signal can be reduced by increasing the dead-time delay (de = 2 ms in this case). A symmetric window function centered at the echo top can be applied to reduce these artifacts while preserving parity between the two halves of the full-echo signal. Fig. 1b illustrates the small wiggles in the imaginary spectrum that can arise from truncation at the beginning of the full-echo signal. These types of distortions have a negligible effect on the indirect *rf* field calibration described here.

Based on the properties of full-echo signals described above, the following procedure is proposed for indirect *rf* field calibration by measuring the Bloch-Siegert shift induced phase change:

1. Acquire a full-echo signal of a setup sample with well resolved ^1H signal(s). The echo delay τ_e needs to be sufficiently long to accommodate the maximum off-resonance pulse length and avoid significant truncation of the echo signal. A longer dead time (de) may be needed if incompletely filtered signal from the refocusing pulse is present at the beginning of the acquisition.
2. Apply a window function such as a sine bell or Gaussian centered at the top of the echo. The aim of the window function is to reduce disparity between the two halves of the full-echo by smoothing out echo truncation or residual signals at the beginning of the acquisition.
3. Estimate the number of dwell intervals for the echo delay $n_{dw} = \tau/dw$, where $\tau \approx \tau_e - \text{de}$, then apply a first-order phase correction PHC1 = 360° $\times$ n_{dw}. The large first-order correction is equivalent to a shift of the time-axis origin near the echo top.
4. Minimize the signal(s) with zeroth-order phasing and fine-tune the zeroth- and first-order phasing interactively to null the peak(s).
5. Add 90° to the zeroth-order phase correction to obtain the real absorptive spectrum.

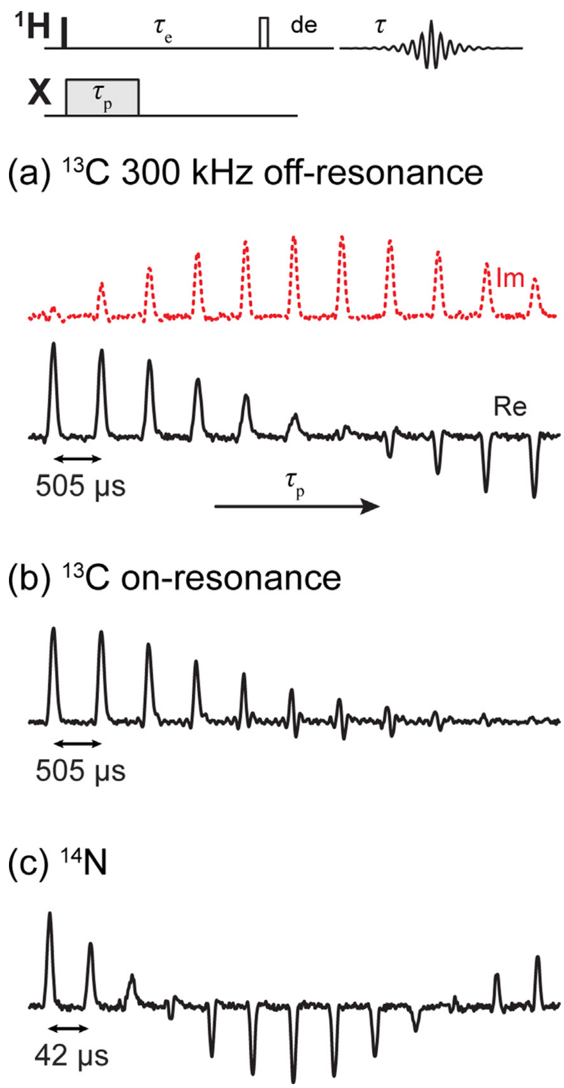

Fig. 2. ^{1}H-detected Bloch-Siegert shift nutation spectra as a function of the pulse length τ_p applied to (a and b) ^{13}C, or (c) ^{14}N *rf* channels. ^{1}H NMR spectra of the CH_3 site of [U-^{13}C, ^{15}N]-L-alanine acquired at 18.8 T and 95 kHz MAS. The ^{13}C pulse carrier frequency was placed 300 kHz off-resonance in (a) and on-resonance in (b). (c) The ^{14}N channel *rf* calibration does not require the presence of ^{14}N nuclei in the sample. The ^{13}C and ^{14}N *rf* fields were calibrated to be 62 and 79 kHz, respectively, from the measured Bloch-Siegert shift using Eq. (10). In (a), the increase in pulse length changes the echo signal phase and consequently mixes the real (black solid trace) and imaginary (red dashed trace) components of the full-echo spectra. In (b), the nutation curve is affected by the CH dipolar recoupling from on-resonance irradiation. (For interpretation of the references to colour in this figure legend, the reader is referred to the web version of this article.)

6. Acquire a series of spectra by increasing the pulse length τ_p and process them using the same window function and phasing parameters determined above.
7. The Bloch-Siegert shift can be measured from the nutation curve from which ν_{1X} can be determined using Eq. (10).

Fig. 2 shows arrays of spectra used to measure the Bloch-Siegert shift and *rf* field. The signal intensity of the full-echo spectrum is modulated by $\cos(2\pi\Delta\nu_{BS}\tau_p)$, from which $\Delta\nu_{BS}$ can be determined. If the applied power is strong enough, then at the null $\Delta\nu_{BS} = 1/(4\Delta\tau_p)$, where $\Delta\tau_p$ is the difference in pulse length between the null spectrum and the first spectrum, which has the maximum intensity. The *rf* field for the X channel $\nu_{1X} = |\gamma_X B_1/2\pi|$ is calculated using the following equation obtained from Eq. (5),

$$\nu_{1X} = \frac{\nu_X}{\nu_H}\sqrt{\nu_H\Delta\nu_{BS}\left(1-\left(\frac{\nu_X}{\nu_H}\right)^2\right)} = \frac{\nu_X}{\nu_H}\sqrt{\frac{\nu_H}{4\Delta\tau_p}\left(1-\left(\frac{\nu_X}{\nu_H}\right)^2\right)} \quad (10)$$

It is important to note that indirect *rf* calibration through the Bloch-Siegert shift does not require the nuclei to be present in the sample. For solid samples, it is actually better to choose a sample without the nucleus of interest so any dipolar recoupling effects induced by the applied *rf* irradiation under MAS can be avoided. In this respect, the pulse sequence used here is actually identical to the TRAPDOR experiment used to measure distances between spin-1/2 and quadrupolar nuclei under MAS [16–18]. Though the applied *rf* field is not selected for any specific recoupling condition, the effect from dipolar coupling is evident when the ^{13}C carrier frequency is on or near resonance (Fig. 2b). The dipolar recoupling can be avoided by placing the ^{13}C frequency far off-resonance as in Fig. 2a.

The ^{13}C signal of [U-^{13}C, ^{15}N]-L-alanine in a 0.75 mm rotor is still strong enough for direct ^{13}C *rf* field measurement via cross-polarization. The pulse lengths used for direct *rf* calibration are typically microseconds long as compared to milliseconds for the indirect method described here. Hence, 'edge effects' can be significant for short pulses and we use the null of a long pulse for the direct measurement when comparing the two methods. For an applied power level of 22.8 W, a ^{13}C *rf* field of ν_{1C} = 62.5 kHz was calibrated using a 990° pulse length after cross-polarization. For the Bloch-Siegert shift method, ν_{1C} = 62 kHz is obtained in good agreement with the direct measurement.

Fig. 2c shows the Bloch-Siegert shift nutation curve for the ^{14}N channel of the probe. The ^{14}N signal is too weak for direct detection due to the small sample amount, low ^{14}N gyromagnetic ratio, large first-order quadrupole broadening, and low *rf* efficiency, which was reduced in the probe circuit to optimize for ^{1}H detection. The indirect Bloch-Siegert method through proton detection is not restricted by these intrinsic limitations. In fact, lower gyromagnetic ratios are more favorable since larger Bloch-Siegert shifts are induced at lower frequencies. For the same ν_{1X}, the Bloch-Siegert shift $\Delta\nu_{BS}$ is proportional to the inverse square of γ_X. The ^{14}N calibration shows a much faster nutation curve than for ^{13}C. With 200 W of power a *rf* field of ν_{1N} = 79 kHz was obtained for the ^{14}N channel.

In conclusion, a robust method for calibrating the *rf* field of insensitive nuclei is presented by which the nucleus of interest does not have to be present in the sample. This is of particular advantage for probes and nuclei for which direct *rf* calibration would be difficult or inconvenient. On the other hand, the indirect calibration of the *rf* field relies on the measurement of a small Bloch-Siegert shift. By using a constant-time spin-echo the effects of T_2 relaxation can be taken into account in the proposed procedure for the *rf* field measurement.

Declaration of Competing Interest

The authors declare that they have no known competing financial interests or personal relationships that could have appeared to influence the work reported in this paper.

Acknowledgements

This work was supported by the National High Magnetic Field Laboratory (USA) through National Science Foundation Cooperative Agreement (DMR-1644779) and by the State of Florida.

References

[1] F. Bloch, A. Siegert, Magnetic resonance for nonrotating fields, Phys. Rev. 57 (1940) 522–527, https://doi.org/10.1103/PhysRev.57.522.

[2] S.H. Autler, C.H. Townes, Stark effect in rapidly varying fields, Phys. Rev. 100 (1955) 703–722, https://doi.org/10.1103/PhysRev. 100.703.
[3] N.F. Ramsey, Resonance transitions induced by perturbations at 2 or more different frequencies, Phys. Rev. 100 (1955) 1191–1194, https://doi.org/10.1103/PhysRev.100.1191.
[4] S.A. Vierkötter, Applications of the Bloch-Siegert shift in solid-state proton-dipolar-decoupled 19F MAS NMR, J. Magn. Reson. A. 118 (1996) 84–93, https://doi.org/10.1006/jmra.1996.0012.
[5] W.A. Anderson, R. Freeman, Influence of a second radiofrequency field on high-resolution nuclear magnetic resonance spectra, J. Chem. Phys. 37 (1962) 85–103, https://doi.org/10.1063/1.1732980.
[6] G. Wider, R.V. Hosur, K. Wüthrich, Suppression of the solvent resonance in 2D NMR spectra of proteins in H20 solution, J. Magn. Reson. 52 (1983) 130–135.
[7] L. Emsley, G. Bodenhausen, Phase shifts induced by transient Bloch-Siegert effects in NMR, Chem. Phys. Lett. 168 (1990) 297–303, https://doi.org/10.1016/0009-2614(90)85614-I.
[8] S. Grzesiek, A. Bax, Correlating backbone amide and side chain resonances in larger proteins by multiple relayed triple resonance NMR, J. Am. Chem. Soc. 114 (1992) 6291–6293, https://doi.org/10.1021/ja00042a003.
[9] R.V. Hosur, R.R. Ernst, K. Wüthrich, A simple two-dimensional measurement of the decoupler power during continuous homonuclear irradiation for the correction of Bloch-Siegert shifts, J. Magn. Reson. 54 (1983) 142–145, https://doi.org/10.1016/0022-2364(83)90153-1.
[10] L.I. Sacolick, F. Wiesinger, I. Hancu, M.W. Vogel, B1 mapping by Bloch-Siegert shift, Magn. Reson. Med. 63 (2010) 1315–1322, https://doi.org/10.1002/mrm.22357.
[11] J.H. Shirley, Solution of Schrodinger equation with a Hamiltonian periodic in time, Phys. Rev. 138 (1965) B979–B987, https://doi.org/10.1103/PhysRev.138.B979.
[12] P. Hannaford, D.T. Pegg, G.W. Series, Analytical expressions for the Bloch-Siegert shift, J. Phys. B. 6 (1973) L222–L225, https://doi.org/10.1088/0022-3700/6/8/009.
[13] W.H. Press, S.A. Teukolsky, W.T. Vetterling, B.P. Flannery, Numerical recipes 3rd edition: the art of scientific computing, third ed., Cambridge University Press, Cambridge, UK New York, 2007.
[14] S.P. Brown, S. Wimperis, Two-dimensional multiple-quantum MAS NMR of quadrupolar nuclei. Acquisition of the whole echo, J. Magn. Reson. 124 (1997) 279–285.
[15] P.J. Grandinetti, J.H. Baltisberger, A. Llor, Y.K. Lee, U. Werner, M.A. Eastman, A. Pines, Pure-absorption-mode lineshapes and sensitivity in 2-dimensional dynamic-angle spinning NMR, J. Magn. Reson. Ser. A. 103 (1993) 72–81.
[16] E.R.H. van Eck, R. Janssen, W.E.J.R. Maas, W.S. Veeman, A novel application of nuclear spin-echo double-resonance to aluminophosphates and aluminosilicates, Chem. Phys. Lett. 174 (1990) 428–432, https://doi.org/10.1016/S0009-2614(90)87174-P.
[17] C.P. Grey, W.S. Veeman, A.J. Vega, Rotational echo 14N/13C/1H triple resonance solid-state nuclear magnetic resonance: A probe of 13C–14N internuclear distances, J. Chem. Phys. 98 (1993) 7711–7724, https://doi.org/10.1063/1.464579.
[18] C.P. Grey, A.J. Vega, Determination of the quadrupole coupling-constant of the invisible aluminum spins in zeolite HY with 1H/27Al Trapdor NMR, J. Am. Chem. Soc. 117 (1995) 8232–8242, https://doi.org/10.1021/ja00136a022.